High-Frequency Bipolar Solid-State LTD Based on a Self-Triggering H-Bridge

Yan Mi, *Senior Member, IEEE*, Ning Xu, Jiacheng Chen, and Zhengmin Li

***Abstract*—In pulsed electromagnetic field tumor ablation, a bipolar nanosecond pulsed electric field has obvious therapeutic advantages. This article proposes a bipolar linear transformer drive (LTD) source circuit topology with a self-triggering H-bridge for this application. In this topology, in the absence of a magnetic core reset circuit, high-frequency bipolar pulse output is realized by introducing an H-bridge while keeping the circuit structure simple. A self-triggered H-bridge is formed by cleverly introducing a self-triggered circuit in the H-bridge, which reduces the difficulty of circuit control. There are only two main control signals, and the sources of all the main control switches share the same ground. The self-triggered switches are self-triggered through the energy-taking capacitor, which improves the stability of the switch control. Theoretical analysis and simulation results demonstrated the theoretical feasibility of the above-mentioned topology; thus, an experimental prototype was built to test the key parameters. The entire prototype adopts a modular design, and each module consists of only four self-triggering H-bridges and one nanocrystalline magnetic core. The key parameters of the final designed prototype are as follows: voltage amplitude of ±4 kV, pulse width of 60–260 ns, pulse rising edge of approximately 11 ns, continuous operation at a maximum frequency of 10 kHz, and output of 500 kHz high-frequency nanosecond pulse.**

***Index Terms*—Bipolar linear transformer drive (LTD), high frequency, magnetic core, pulse generator, self-triggering.**

I. Introduction

IN RECENT years, the use of high-voltage pulsed electric fields to induce irreversible electroporation for tumor tissue ablation has entered the stage of clinical trials and shown good therapeutic effects [1]–[4]. trains Relevant studies have shown that bipolar pulsed electric field can induce irreversible electroporation [5], with good uniformity in the treatment of tumors, and effectively inhibit muscle contraction [6]–[8]; thus, this method has good application prospects. Therefore, the development of a high-frequency bipolar pulse generator is highly desirable for its application in the biomedical field.

Most bipolar pulse generators have evolved from inverter circuits. Therefore, the most direct way to generate bipolar pulses is to use H-bridges to directly chop the high-voltage power supply [9]. This method requires multiple solid-state switches in series to form a bridge arm to output a sufficiently high voltage pulse on the load side. However, because this topology has no boost function, it requires an expensive high-voltage dc power supply. In addition, because the switch parameters cannot be made completely consistent, they also involve complex switch voltage equalization problems [10], [11]. There are also researchers who use the H-bridge chopper unipolar Marx circuit to achieve bipolar pulse voltage output [12]–[14], which solves the voltage boost problem, but this method also requires a voltage equalization circuit, which will increase the complexity of the system and the risk of system failure.

To solve the above-mentioned problems, some scholars have analogized the Marx circuit structure and connected multistage bridge circuits in series to achieve bipolar pulse output [15], [16]. The output of the H-bridge at all levels of this circuit is independent and does not share the ground. Therefore, it is necessary to use a multichannel isolated output high-voltage dc power supply or an auxiliary charging switch to charge the capacitor. Furthermore, the circuit has a large number of switches and is complex to control. To reduce the number of switches in the circuit and reduce the difficulty of circuit control, some scholars have made appropriate improvements to the H-bridge series structure and introduced inductive isolation charging [17]. However, it is still necessary to control the action of the corresponding switch to realize the charging of the energy storage capacitor, which will increase the switching loss of the switch and is unfavorable for the high frequency operation of the circuit [18]. In addition, some researchers directly cascade the output of positive and negative Marx circuits to obtain bipolar pulse output [19], but they also face the problems of more circuit modes and complex control.

In recent years, modular multilevel converter topologies have also been widely used to generate high-voltage bipolar pulses [20]. However, this topology also needs to control the corresponding switch to provide a charging circuit for the energy storage capacitor. Therefore, when it is necessary to output a higher pulse frequency, the switching loss of the circuit increases sharply, which seriously threatens the normal operation of the switch. The bipolar pulse-forming line generator can only adjust the pulse width by changing the length of the transmission

Manuscript received July 17, 2021; revised October 21, 2021; accepted November 19, 2021. Date of publication December 1, 2021; date of current version January 19, 2022. This work was supported in part by the National Natural Science Foundation of China under Grant 52077022 and in part by 111 Project under Grant BP0820005. Recommended for publication by Associate Editor A. Trzynadlowski. *(Corresponding author: Ning Xu.)*

Yan Mi, Jiacheng Chen, and Zhengmin Li are with the State Key Laboratory of Power Transmission Equipment & System Security and New Technology, Chongqing University, Chongqing 400044, China (e-mail: miyan@cqu.edu.cn; 20181102016t@cqu.edu.cn; 202011131193@cqu.edu.cn).

Ning Xu is with the State Key Laboratory of Power Transmission Equipment & System Security and New Technology, Chongqing University, Chongqing 400044, China, and also with the State Grid Shanghai Municipal Electric Power Company, Shanghai 200122, China (e-mail: xuning@cqu.edu.cn).

Color versions of one or more figures in this article are available at https://doi.org/10.1109/TPEL.2021.3131251.

Digital Object Identifier 10.1109/TPEL.2021.3131251

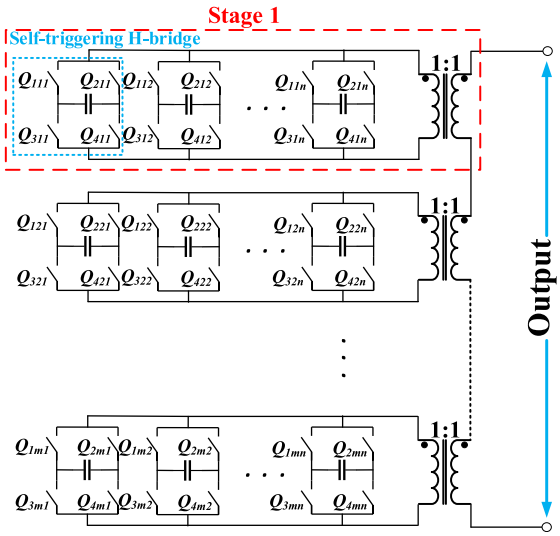

Fig. 1. Schematic diagram of m-stage SH-B-LTD.

line and requires load impedance matching with poor flexibility [21]. [22] The characteristics of various types of bipolar pulse generators are listed and summarized, and the control systems of most bipolar generators are complicated.

In the linear transformer drive (LTD), the control of the switches is simple and reliable because the sources of all switches are common ground. An LTD module generally uses a multibranch parallel discharge structure [23]–[25], which is very suitable for generating fast-changing short pulses. However, due to the saturation effect of the magnetic core, the conventional unipolar LTD must introduce an active reset circuit [26]. This increases the complexity of the generator, limits the output pulse width of the generator, and causes the operating frequency of the LTD to not be too high. Additionally, the electromagnetic interference of bipolar LTDs is strong, and control is difficult. At present, the research on bipolar LTDs is rare.

To meet the needs of biological applications and support bipolar LTD research, in this article, a self-triggering H-bridge circuit is cleverly introduced into the conventional unipolar LTD topology, and a novel solid-state bipolar LTD is designed. The entire generator adopts a modular design, and the source of the main control switch shares the ground, thereby retaining the basic advantages of LTDs, and the circuit has fewer operating modes and simple control.

In this article, we first describe the circuit topology and working principle of the generator. Then, PSpice is used for simulation analysis, and the simulation results verify the theoretical feasibility of the topology. Finally, a self-triggering H-bridge (SH-B-LTD) prototype is designed, the key parameters of the prototype are tested, and the practicability of the topology is verified.

II. Topology and Operation of the Proposed SH-B-LTD

A schematic diagram of the m-stage SH-B-LTD circuit in this article is shown in Fig. 1. This article considers a modular design, and the working processes of each self-triggered

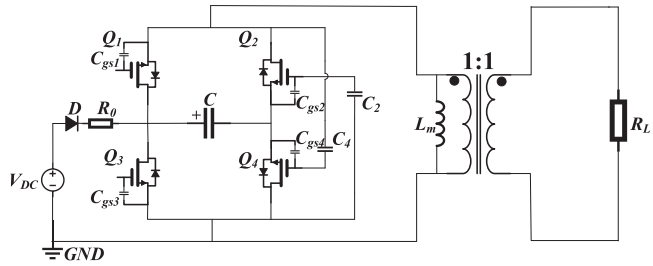

Fig. 2. SH-B-LTD topology.

H-bridge in each module are completely the same. Therefore, for the convenience of introduction, the following introduces only the working process of a single self-triggered H-bridge in Fig. 1. The stray parameters in the actual circuit are ignored and only the magnetizing inductance of the transformer is considered. Moreover, the corresponding equivalent circuit is shown in Fig. 2. In the figure, L_m is the magnetizing inductance of the 1:1 transformer, C is the energy storage capacitor, C_{gsn} is the gate–source junction capacitance of the switch, C_2 and C_4 are the energy-taking capacitors of the switch gate, D and R_0 are the charging isolation diode and isolation resistance, and R_L is the load resistance.

In this topology, the source of switches Q_1 and Q_3 has zero dc potential to the ground. In the face of the relatively strong electromagnetic interference in the bipolar LTD, switch source grounding can improve the stability of the control and improve the reliability of switch operation. Switches Q_2 and Q_4 can be self-triggered through the energy-taking capacitor. Next, the working process of the circuit will be described in detail.

A. Mode I

The generator works in charging mode, as shown in Fig. 3(a). At this time, all the switches are inoperative, and the high-voltage dc power supply charges the energy-storage capacitor C through the charging resistor and parasitic diode of switch Q_4. When the steady state is reached, the voltage of the energy storage capacitor is equal to the charging voltage $V_{\rm dc}$.

B. Mode II

The generator works in positive discharging mode. First, the resistive load is taken as an example, as shown in Fig. 3(b). Switch Q_1 is turned ON by the active control signal, and the generator has no output pulse at this time. Subsequently, the energy-storage capacitor C will charge the gate-source junction capacitance C_{gs4} of switch Q_4 through switch Q_1 and energy-taking capacitor C_4. When the voltage across C_{gs4} reaches the threshold voltage of the switch, switch Q_4 is turned ON, and the generator starts to output a positive polarity pulse. Then, the gate-source voltage of Q_4 continues to rise until the sum of the gate-source voltage of the switch and the voltage of the divider capacitor is equal to the voltage of the energy storage capacitor. The turn-ON process of Q_4 is completed, and the generator stably outputs a pulse voltage with an amplitude of $V_{\rm dc}$. Then, if multiple identical self-triggering H-bridges are output in parallel, the

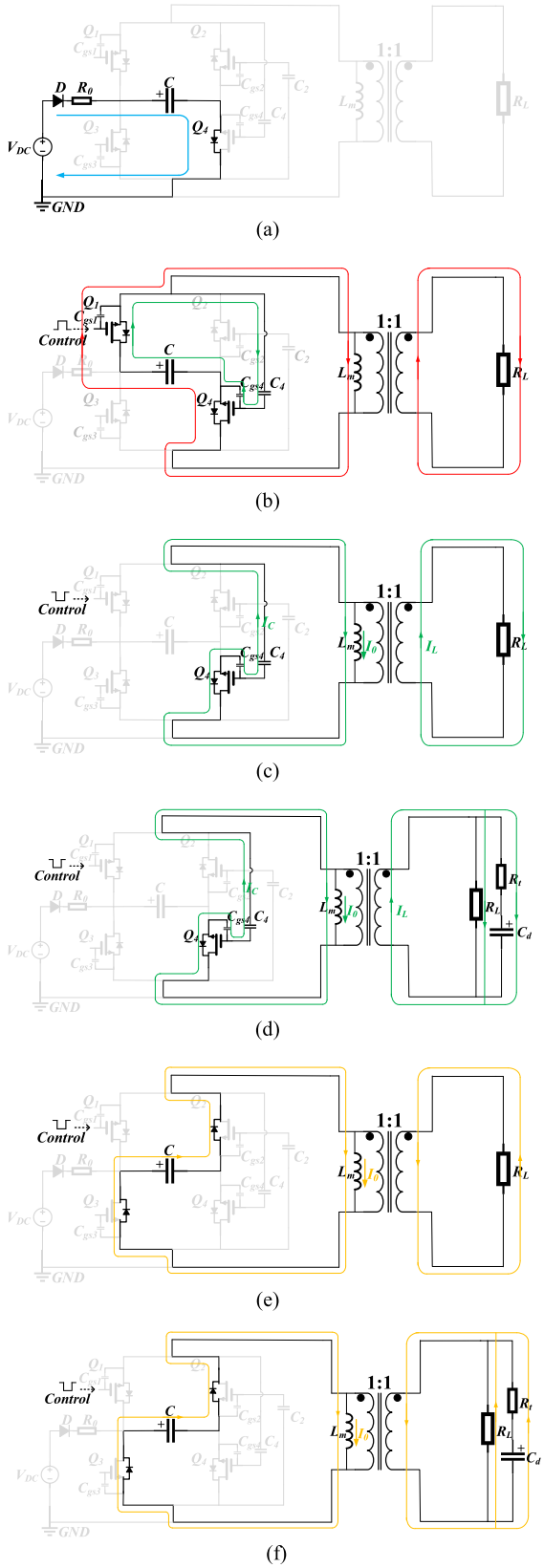

Fig. 3. (a) Charging mode. (b) Positive discharging mode under a resistive load. (c) Turn-OFF mode under a resistive load. (d) Turn-OFF mode under a capacitive load. (e) Magnetic core energy transfer mode under a resistive load. (f) Magnetic core energy transfer mode under a capacitive load.

equivalent stray inductance can be reduced, thereby reducing the rise time of the output pulse. If m identical SH-B-LTD modules are superimposed, the pulse voltage of mV_{dc} can be output.

Although biological tissue is a resistive-capacitive load [27], Fig. 3(b) shows that the self-triggering process of the switch is not affected by the load type since there is no direct electrical coupling between the self-triggering circuit and the load. That is, we can consider that the resistive-capacitive load and the resistive load are consistent.

C. Mode III

This mode describes the shutdown process of the generator. A resistive load is shown in Fig. 3(c). Switch Q_1 is controlled and turned OFF by an active control signal. Energy-storage capacitor C stops discharging, but the output voltage of the generator does not disappear. Then, the junction capacitance of switch Q_4 begins to discharge through the C_{gs4}-C_4 transformer primary-Q_4 loop, and the output pulse amplitude begins to decrease. When the discharge reaches the cutoff voltage of Q_4, switch Q_4 turns OFF. Note that the time constant of the discharge path in this process is slightly larger than the time constant of the charge path (C–C_4–C_{gs4}), so the turn-OFF time of the switch is slightly longer than the turn-ON time.

In addition, the discharge current Ic of C_{gs4} is composed of the excitation current I_0 and the load current I_L. When R_L and L_m remain the same, if the input voltage V_{dc} is constant (I_L is constant), the wider the pulse width is, the larger the corresponding I_0, i.e., the shorter the turn-OFF time of the switch.

The actual biological tissue equivalent circuit in [27], adding a resistance–capacitance load branch, is shown in Fig. 3(d). Introduction of the resistance–capacitance load branch will have a certain impact on the size of I_L (relative to the resistance load), so it will affect the turn-OFF speed of the switch to a certain extent. Fortunately, the size of I_0 is only related to V_{DC} and pulse width. Therefore, the change in I_L has little effect on the turn-OFF process of the switch.

D. Mode IV

This mode describes the transfer of stored energy (that is, the current "I_0") in the magnetic core. A resistive load is shown in Fig. 3(e). After switch Q_4 is turned OFF, the current in the circuit is not be immediately reduced to zero due to the energy stored in the magnetic core. The energy stored in the magnetic core is divided into two parts and gradually transferred. One part is transferred to the energy storage capacitor through the parasitic diodes of switches Q_2 and Q_3. The other part is consumed in the load. After the stored energy is completely transferred, the magnetic core returns to its remanence point. During this process, the magnetic core energy consumed on the load causes a certain negative pulse voltage to appear across the load resistance, and this negative pulse voltage begins to appear from the moment *mode IV* begins.

During this process, all switches are turned OFF. Therefore, when the circuit is connected in parallel with the resistance–capacitance load branch [see Fig. 3(f)], the working process

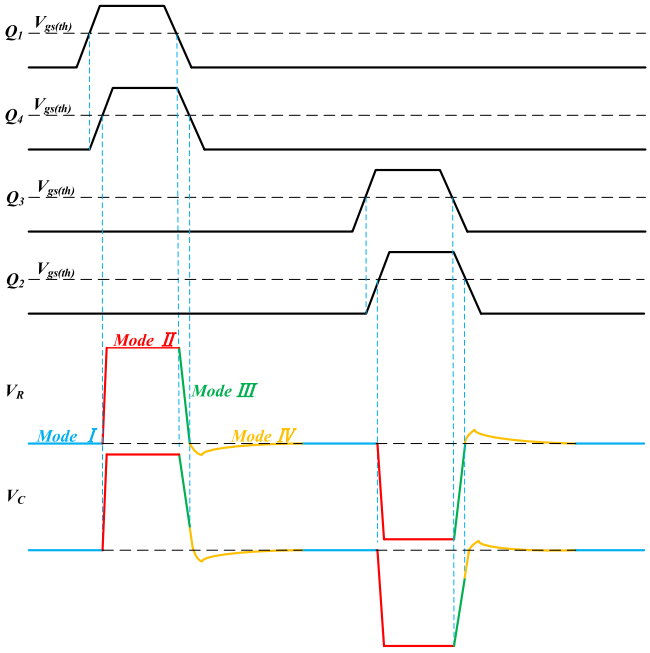

Fig. 4. Timing diagram of the switching signal and pulse output waveform.

of the circuit is almost the same as the working process of a resistive load. However, note that at the beginning of mode IV, the polarity of the output voltage is not reversed immediately because a certain amount of energy is stored on capacitor C_d, which is somewhat different from a resistive load.

The above-mentioned four modes are repeated in subsequent steps. When mode II controls the switching action of switch Q_3 through the active control signal and the subsequent mode III is the passive triggering of switch Q_2 through energy-taking capacitor C_2, the circuit outputs a negative pulse voltage. The other working process is exactly the same as the positive polarity, so the explanation is not repeated here.

In summary, the timing diagram of the switching signal and pulse output waveform of the whole working process is shown in Fig. 4. In the figure, V_R is the output waveform under a resistive load, and V_C is the output waveform under a capacitive load.

III. Parameter Selection

This article considers building a five-stage SH-B-LTD prototype with a maximum charging voltage of 800 V and four self-triggering H-bridges embedded in each stage of the module.

According to the previous analysis, selection of the energy-taking capacitor has a large influence on the reliable operation of the self-triggering switch. In the gate trigger circuit of Fig. 5, C is much larger than C_{gs4}; thus, the energy storage capacitor can be regarded as an ideal voltage source. Therefore, the equivalent gate trigger circuit after considering the stray parameters is shown in Fig. 6, where L_{s4} represents the total stray inductance of the trigger loop and R_{g4} is the drive resistance.

In fact, the essence of the MOSFET turn-ON process is the dynamics of charge redistribution from the gate capacitor to the

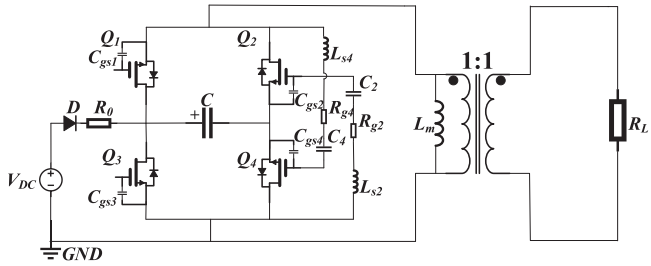

Fig. 5. SH-B-LTD topology considering stray inductance parameters.

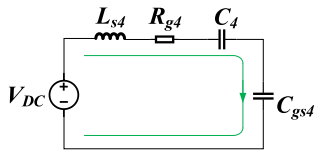

Fig. 6. Q_4 equivalent gate trigger circuit.

gate–source capacitor of each MOSFET. The working process of the SiC FET is similar to that of the MOSFET [28], [29]. According to the conservation of charge principle, energy-taking capacitor C_4 must satisfy the following relationship [30]:

$$C_{4(\min)} = \frac{Q}{\Delta U} = \frac{U_{gs(th)}C_{gs4} + (U_{gs(th)} + U_{ds4(\mathrm{OFF})})C_{gd4}}{U_C - U_{gs(th)}} = \frac{U_{gs(th)}C_{gs4} + U_{gs(th)}C_{gd4}}{U_C - U_{gs(th)}} \tag{1}$$

where $U_{gs(th)}$ and $U_{ds4(\mathrm{OFF})}$ represent the threshold voltage of Q_4 and the drain-source voltage in the OFF- state, respectively. In the topology of this article, $U_{ds4(\mathrm{OFF})} = 0$. Moreover, a threshold voltage margin factor α is defined, which satisfies

$$C_{4(\max)} = \frac{\alpha U_{gs(th)}C_{gs4} + U_{gs(th)}C_{gd4}}{U_C - U_{gs(th)}} \tag{2}$$

where $U_{gs4(set)} = \alpha U_{gs(th)} \leq U_{gs4(\max)}$. At this time, the value range of capacitor C_4 is determined by the following formula:

$$C_{4(\min)} \leq C_4 \leq C_{4(\max)}. \tag{3}$$

In fact, the circuit shown in Fig. 6 is a typical *RLC* oscillator circuit. To ensure the switching speed of the switch and prevent a large voltage overshoot of the switch, the *RLC* oscillation circuit is generally controlled to work in a critically damped state. The driving resistance R_{g4} satisfies the following expression:

$$R_{g4} = 2\sqrt{\frac{L_{s4}}{C_{gs4}}\left(1 + \frac{C_{gs4}}{C_4}\right)}. \tag{4}$$

With (1)–(4), combined with the actual parameters of the switch, this article finally selects a chip capacitor with a withstand voltage of 1000 V and a capacitance value of 15 pF as the energy-taking capacitor. To ensure the switching speed and reduce the oscillation of the drive waveform of the self-triggered switch as much as possible, the drive resistance value is taken as 4.7 Ω.

TABLE I
MAIN EQUIPMENT ON EACH STAGE OF LTD MODULE

Device	Model	Parameter
SIC FET	UF3C120080B7S	1200V, 28A
energy-taking capacitor	C1206C150JDGACAUTO	1000V, 15pF
magnetic core	1K107	70mm×40mm×25mm
energy-storage capacitor	C4AQPLU4170M12J	1200V, 1.7μF

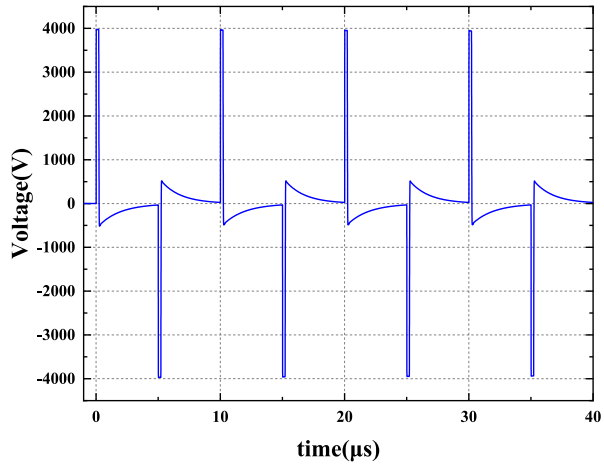

Fig. 7. (a) Bipolar output with a frequency of 100 kHz and pulse width of 220 ns. (b) Positive output with different pulse widths.

IV. SIMULATION RESULTS

To verify the theoretical feasibility of the SH-B-LTD (see Fig. 1) proposed in this article, combined with the circuit topology shown in Fig. 1, the device parameters selected in Table I are used to build a simulation model in PSpice software for simulation analysis. In addition, note that SH-B-LTD has five stages, and each stage has four self-triggering H-bridges in parallel; i.e., m = 5 and n = 4. A pure resistance load of 500 Ω is used to replace the biological tissue to be treated, and $V_{\rm dc}$ = 800 V.

The output result of the simulation is shown in Fig. 7. The simulation results show that the circuit topology can output symmetrical bipolar pulse voltages with frequencies of 100 kHz. Additionally, Fig. 7(a) shows that the amplitude of the output waveform is 4 kV. After each pulse, there is a reverse pulse voltage lasting approximately 5 μs. This voltage is caused by part of the energy stored in the magnetic core being discharged in the load resistance, which is consistent with mode IV in the theoretical analysis.

Keeping other parameters unchanged and changing only the pulse width, the output result of a single positive pulse is shown in Fig. 7(b). It is not difficult to see that the fall time of the pulse is indeed longer than the rise time, and the wider the pulse is, the steeper the falling edge. This corresponds to the analysis of mode III.

In summary, the feasibility of the SH-B-LTD topology proposed in this article is verified by simulation.

V. EXPERIMENTAL RESULTS

A. Construction of the Experimental Platform

This article uses the devices selected in Table I to complete the construction of a five-stage SH-B-LTD prototype. To reduce the size of the generator, this article uses a four-layer PCB as the main board of each stage of the LTD module. Moreover, to ensure the symmetry of the circuit and the current shared between the respective self-triggering H-bridges, the PCB board is designed to be circular, and all the components are soldered on a circular PCB board with a radius of 12 cm. The front of the PCB board mainly includes control circuits, active control switches, energy storage capacitors, and charging isolation resistors. The physical diagram is shown in Fig. 8(a). The back of the PCB board mainly includes self-triggering switches and energy-taking circuits. Finally, the same five-stage LTD modules are connected from bottom to top through copper pillars to complete the construction of a five-stage LTD. The output of the generator is led out through a large copper column on the central axis of each stage module and then connected to a load through an external copper sheet. The final five-stage SH-B-LTD prototype is shown in Fig. 8(b).

The main measurement tools are an oscilloscope (DPO4054, Tektronix, USA), a high-voltage probe (PPE, 5 kV, 400 MHz, LeCroy, USA), a high-voltage differential probe (P5200 A, 1.3 kV, 50 MHz, Tektronix, USA), and a current sensor (2877, 100 A, 200 MHz, Pearson, USA). In addition, a dc power supply (DW-P302-35F5D, Tianjin Dongwen, China) is used to charge the energy storage capacitor with a dc voltage of 3000 V and a current of 35 mA.

B. Key Parameter Test

If there is no special instructions, during the test, a load of the generator is 500 Ω noninductive resistance. The generator was pressurized 800 V per stage, the pulse width was 220 ns, and the repetition frequency was 10 kHz.

1) Switch Drive Waveform Test: The driving waveform of the switch can reflect the working state of the self-triggered H-bridge. The typical driving waveform of the discharge switch in the test of the self-triggered H-bridge is shown in Fig. 9(the

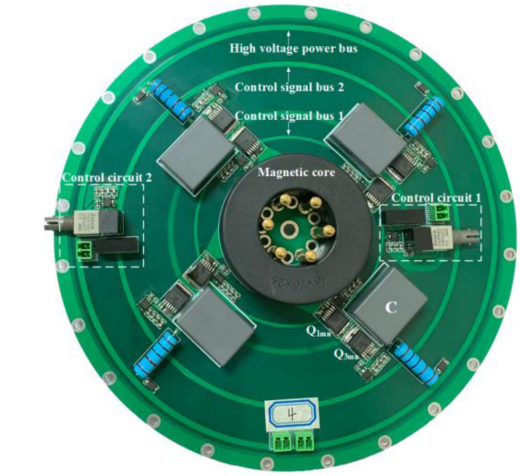

(a)

(b)

Fig. 8. (a) Front view of the SH-B-LTD module. (b) Physical image of the five-stage SH-B-LTD module with a resistive load.

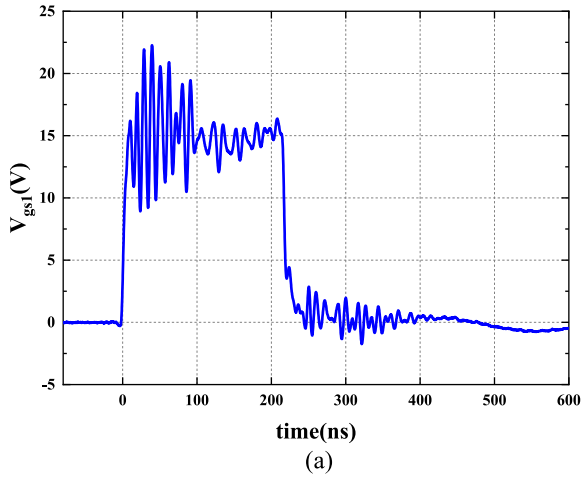

(a)

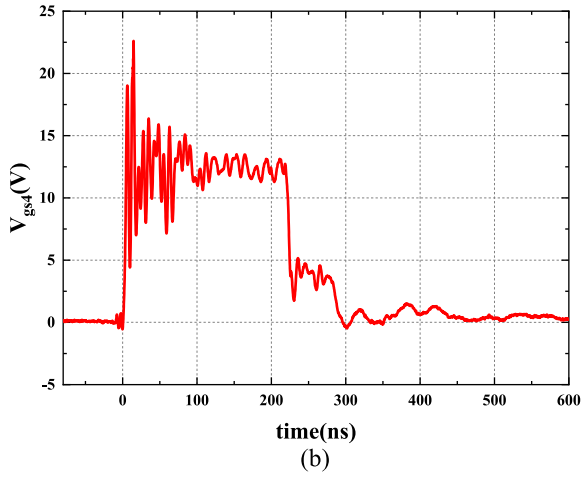

(b)

Fig. 9. (a) Actively controlling the driving waveform of switch Q_1. (b) Driving the waveform of self-triggering switch Q_4.

measuring equipment is P5200A). Due to the existence of stray inductance and distributed capacitance in the actual circuit, the driving voltage waveform of the switch after the addition of the driving resistance still oscillates in the early period of the pulse. However, the maximum value does not exceed 25 V, and the switch can work normally without gate breakdown. The oscillation centers of the driving voltage of the active control switch and the self-triggered switch are 15 V and 12 V, respectively, namely, $U_{gs1(\mathrm{set})} = 15$ V and $U_{gs4(\mathrm{set})} = 12$ V, which meets the design requirements. In addition, note that when the pulse output ends, the voltage U_{ds} at both ends of each switch will change rapidly. This will cause charge transfer in the junction capacitance of the switch. Additionally, a part of the charge will be transferred to the input capacitance through the Miller capacitance of the switch, which will cause a certain voltage rise in U_{gs4}. Fortunately, the amplitude of the rebound voltage is not enough to trigger the switch and will not affect the working process of the circuit.

2) Output Waveform Test: After ensuring that the drive waveform of the switch is normal, the relevant test of the output waveform of the prototype was performed. The output pulse width of the generator was changed by controlling the ON-duration of the active control switch in the self-triggered H-bridge. The output waveform of the prototype under different pulse width conditions is shown in Fig. 11. The test results show that the generator can stably output bipolar pulses with different pulse widths. The rise time of the positive and negative output pulses is only 11 ns, and the voltage transmission efficiency of the generator is as high as 97%. This is because there are four self-triggering H-bridges in parallel in the SH-B-LTD module, and the stray inductance of the circuit during discharge is very small. The falling edge of the pulse becomes faster as the pulse width becomes longer, which is consistent with the simulation result in Fig. 7(b). Moreover, because of the rapid rise in the pulse and the distributed capacitance (mainly caused by the copper coating on the PCB board, which is equivalently connected in parallel to the output end of the generator, as shown in C_B in Fig. 10) that exists in the prototype, the two together lead to the front oscillation of the measured output pulse.

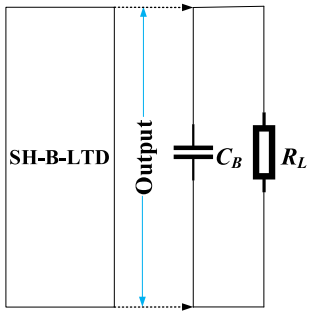

Fig. 10. Distributed capacitance of the generator.

The reliability of the generator working at high frequencies is illustrated. The generator is operated in a pulse train of 100 kHz. The test results are shown in Fig. 12(a), and the waveform profile is almost the same as the simulated waveform. The figure shows that when working at high frequencies, the generator output waveform shows very little distortion and has good repeatability.

Subsequent testing of the limited operating frequency of the generator is conducted while keeping other parameters unchanged and increasing the pulse train frequency of the generator to 500 kHz (the number of pulses in the train is 6). The test results are shown in Fig. 12(b), and the output waveform of the generator still has good repeatability.

The above-mentioned test results show that the generator in this article can stably output high-frequency nanosecond pulses.

3) Excitation Current Test: To show that the working mode of the generator in this article is beneficial to the high-frequency operation of the magnetic core, the excitation current waveform of the magnetic core in the 500 kHz pulse train working modes of the single-stage generator is tested. The results are shown in Fig. 13, and the red arrow points to the start time of the corresponding pulse. To facilitate the description of the working conditions of the magnetic core, Fig. 14 shows the hysteresis loop of the nanocrystalline magnetic core used in this article: $\Delta B_+ = \Delta B_{100k\text{-}} = \Delta B_{500k\text{-}}$.

Fig. 13 shows that for a 500 kHz pulse train, the negative pulse begins to be output (the excitation current begins to change rapidly in the opposite direction) when the excitation current of the positive pulse has not been reduced to 0. At this time, the corresponding hysteresis loop is as follows: The magnetic core changes from $-B_r$ to B_s when the positive polarity pulse is output. The negative-polarity pulse starts to output when the magnetic core returns to point B_x between B_r and B_s, and then, the magnetic flux density changes by $-\Delta B_{500k\text{-}}$. In Fig. 14, the average slope of the $\Delta B_{500k\text{-}}$ segment hysteresis loop is clearly greater than that of the ΔB_+ segment, so the average permeability at a 500 kHz negative polarity discharge is greater, and the excitation current at a negative polarity output is smaller than that of the positive polarity output in Fig. 13. At this time, the envelope area of the hysteresis loop in one cycle is smaller (compared with the magnetic core changes $-\Delta B_{100k\text{-}}$ when the negative polarity pulse is output), so the magnetic core loss is lower. Therefore, the bipolar working mode of the generator can ensure that the magnetic core works in an area with large magnetic permeability and reduce the magnetic core loss during high-frequency operation.

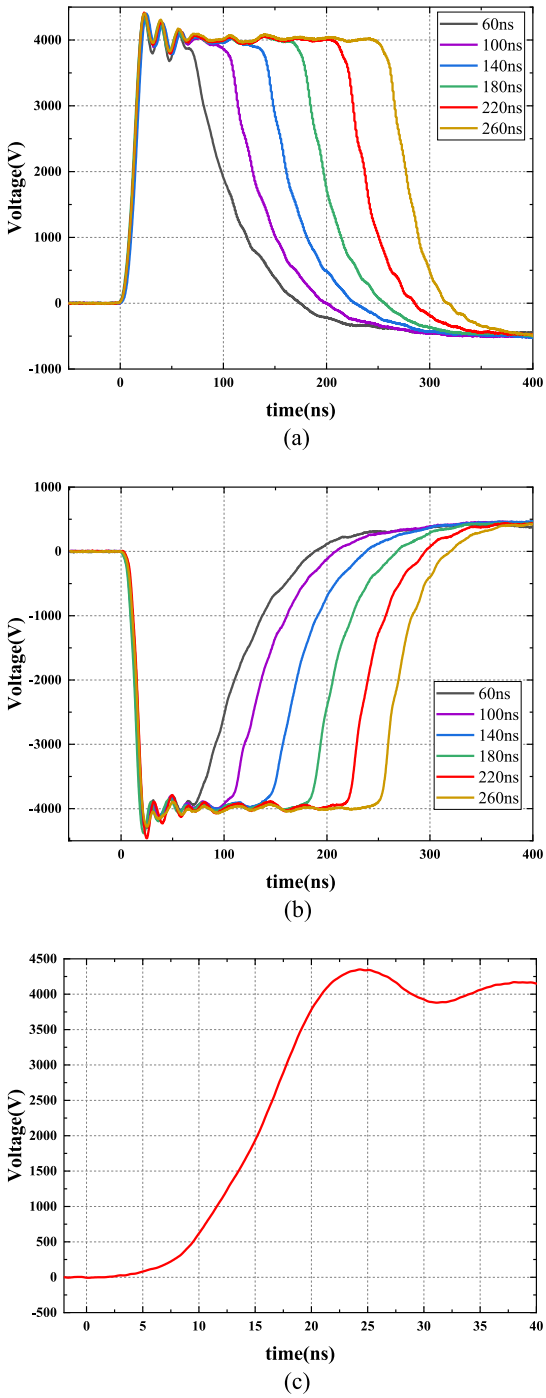

Fig. 11. (a) Positive output waveforms with different pulse widths. (b) Negative polarity output waveforms with different pulse widths. (c) Rising edge of the positive output.

C. Output Waveform Test Under Different Loads

The previous test has shown that the generator can drive a 500 Ω resistance load normally. However, in tumor treatment, the equivalent load resistance value may be less than 500 Ω, which may correspond to a capacitive load. To test the generator's

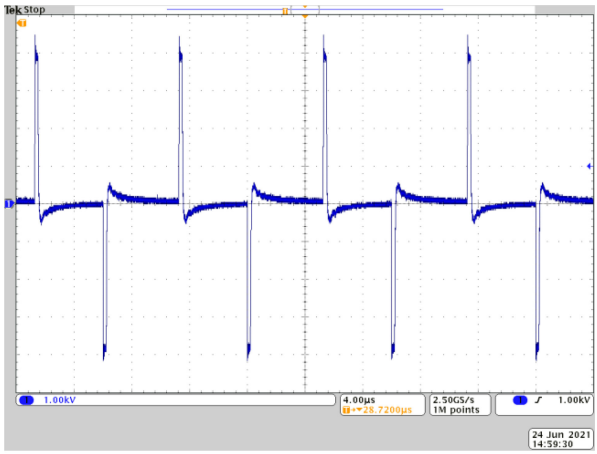

(a)

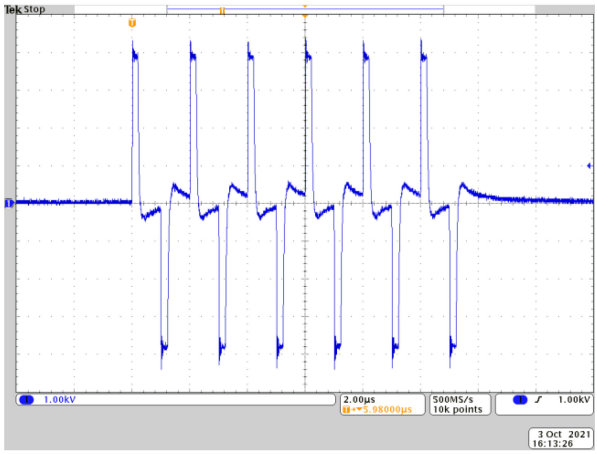

(b)

Fig. 12. (a) Output waveform of a 100 kHz. (b) Output waveform of a 500 kHz.

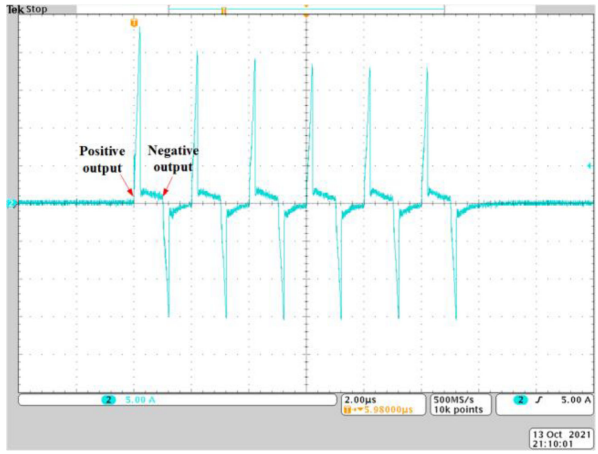

Fig. 13. 500 kHz excitation current waveform.

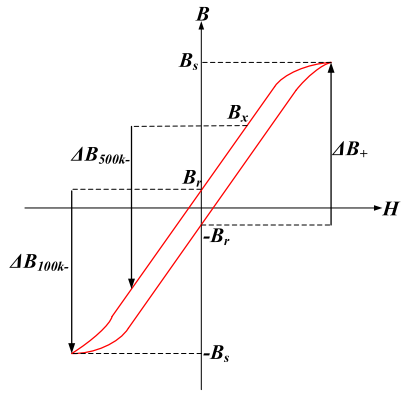

Fig. 14. Hysteresis loop of the nanocrystalline magnetic core.

ability to drive different loads, we tested the output waveform of the generator under different loads.

First, we test the output waveform of the generator under different resistance loads (all noninductive resistance), and the test results are shown in Fig. 15(a). The figure shows that the change in the load resistance has little effect on the leading edge of the pulse. However, it has a greater impact on the trailing edge of the pulse. The smaller the resistance is, the faster the trailing edge of the pulse. This can be explained by the analysis process in mode III; the resistance value decreases, which is equivalent to increasing the value of I_L. As a result, the discharge speed of the gate capacitance of the self-triggering switch is increased, and the turn-OFF speed of the switch increases. In addition, when the resistance is small, the discharge speed of the distributed capacitance (see C_B in Fig. 10) at the output of the generator will increase.

Then, we parallel a capacitive branch ($R_t = 1200\ \Omega$ and $C_d = 1$ nF) at both ends of the 500 Ω resistance load and use the load at this time to simulate actual biological tissue. The voltage and current waveforms output by the generator are shown in Fig. 15. In Fig. 15(a), the falling edge of the pulse after it is incorporated into the capacitive branch is slightly slower, but it does not affect the rising edge of the pulse. This corresponds to the analysis of mode III and mode II. In Fig. 15(b), when the capacitive branch current starts to reverse, all switches have been opened, and the circuit enters mode IV. However, at this time, because the 1 nF capacitor of the capacitive branch has a certain amount of energy stored, the voltage across the load is not immediately reversed (as shown in Fig. 15(c); when the load is purely resistive, it reverses almost at the same time, and the short time delay is caused by distributed capacitance.).

The above-mentioned test results show that the generator in this article can normally drive resistive loads and capacitive loads of different sizes.

In general, the experimental results prove the feasibility and practicability of the topology shown in Figs. 1 and 2, and the high-frequency nanosecond pulse trains generated by SH-B-LTD can basically meet the needs of irreversible electroporation ablation. For some tumor ablation applications that require higher pulse voltages, we can consider increasing the number of generator stages. In theory, this topology can indefinitely increase the number of generator stages. If the equivalent resistance of the biological tissue to be ablated is small, consider increasing the number of self-triggering H-bridges in parallel in each stage to increase the current-carrying capacity of the generator.

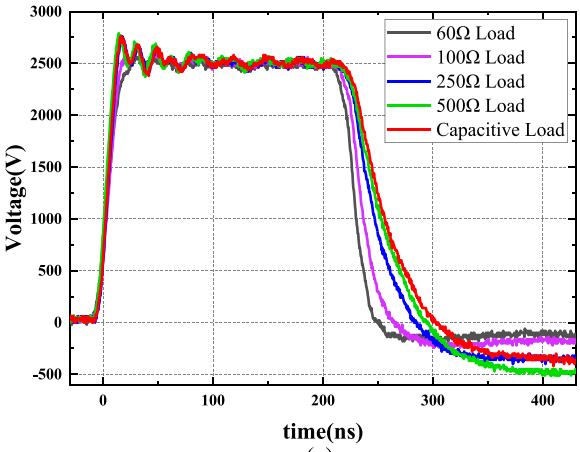

(a)

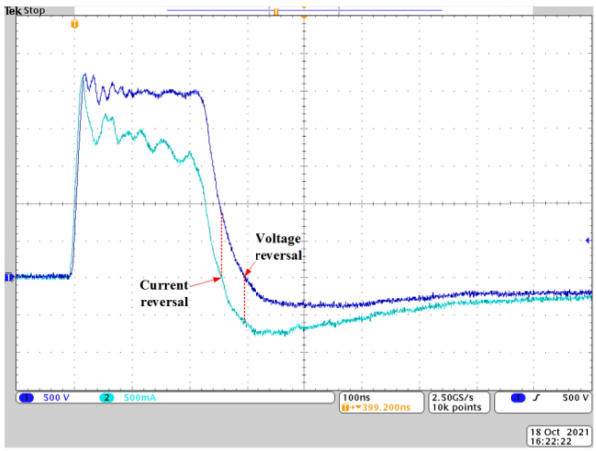

(b)

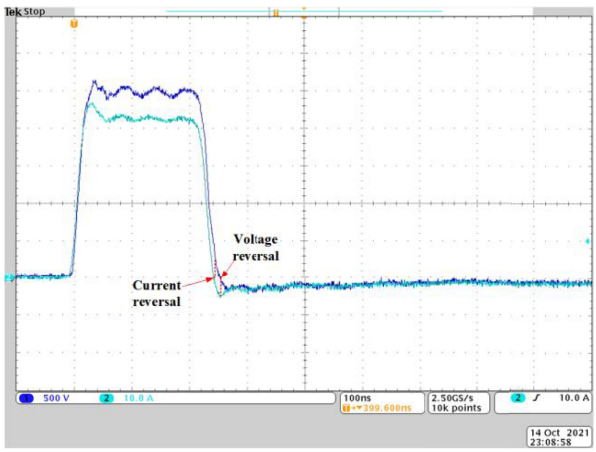

(c)

Fig. 15. (a) Output under different loads. (b) Voltage and current waveforms of the capacitive branch. (c) Voltage and current waveform under a 60 Ω resistive load.

However, note that the falling edge of the generator's output waveform will be affected to a certain extent by the pulse width and the size of the load impedance. This is a shortcoming of SH-B-LTD, and follow-up research should focus on how to remove this influence.

VI. Conclusion

In this article, a new type of SH-B-LTD that can be used in biomedical applications is proposed. It has good clinical application prospects for the irreversible electroporation ablation of tumors. The main conclusions are as follows.

1) By introducing the H-bridge, this topology can achieve high-frequency bipolar operation without the use of active demagnetization circuits. The bipolar working mode can also ensure that the magnetic core works in the region of high magnetic permeability, reduces core loss, increases the utilization rate of the magnetic core, and prevents the problem of magnetic core saturation.
2) By introducing a self-triggering circuit in the H-bridge, the control difficulty of the generator is reduced, and the main control signal is only two channels. The sources of all active control switches are grounded, and the self-triggering switch is passively triggered by an energy-taking capacitor, which is beneficial to adapt to the strong electromagnetic interference environment in the bipolar LTD.
3) This topology can stably output high-frequency bipolar high-voltage nanosecond pulses without isolating the circuit. The voltage amplitude of the five-stage SH-B-LTD prototype is as high as ±4 kV, the pulse rising edge is approximately 11 ns, the pulse width is continuously adjustable within 60–260 ns, the continuous operating frequency is up to 10 kHz, and a high frequency pulse train of 500 kHz can be output.

References

[1] J. F. Edd, L. Horowitz, R. V. Davalos, L. M. Mir, and B. Rubinsky, "In vivo results of a new focal tissue ablation technique: Irreversible electroporation," *IEEE Trans. Biomed. Eng.*, vol. 53, no. 7, pp. 1409–1415, Jul. 2006.

[2] C. Jiang, R. V. Davalos, and J. C. Bischof, "A review of basic to clinical studies of irreversible electroporation therapy," *IEEE Trans. Biomed. Eng.*, vol. 62, no. 1, pp. 4–20, Jan. 2015.

[3] S. Wu, Y. Wang, J. Guo, Q. Chen, J. Zhang, and J. Fang, "Nanosecond pulsed electric fields as a novel drug free therapy for breast cancer: An in vivo study," *Cancer Lett.*, vol. 343, no. 2, pp. 268–274, Feb. 2014.

[4] H. Sarnago, Ó. Lucía, A. Naval, J. M. Burdío, Q. Castellví, and A. Ivorra, "A versatile multilevel converter platform for cancer treatment using irreversible electroporation," *IEEE J. Emerg. Sel. Topics Power Electron.*, vol. 4, no. 1, pp. 236–242, Mar. 2016.

[5] C. Yao *et al.*, "Targeted cell membrane damage by bipolar high repeated frequency pulses," *IEEE Trans. Dielectr. Elect. Insul.*, vol. 24, no. 5, pp. 3270–3282, Oct. 2017.

[6] C. Yao *et al.*, "Bipolar microsecond pulses and insulated needle electrodes for reducing muscle contractions during irreversible electroporation," *IEEE Trans. Biomed. Eng.*, vol. 64, no. 12, pp. 2924–2937, Dec. 2017.

[7] S. Dong, C. Yao, Y. Zhao, Y. Lv, and H. Liu, "Parameters optimization of bipolar high frequency pulses on tissue ablation and inhibiting muscle contraction," *IEEE Trans. Dielectr. Elect. Insul.*, vol. 25, no. 1, pp. 207–216, Feb. 2018.

[8] D. C. Sweeney *et al.*, "Quantification of cell membrane permeability induced by monopolar and high-frequency bipolar bursts of electrical pulses," *Biochimica et Biophysica Acta (BBA) - Biomembranes*, vol. 1858, no. 11, pp. 2689–2698, Nov. 2016.

[9] C. Yao, S. Dong, Y. Zhao, Y. Zhou, Y. Mi, and C. Li, "High-frequency composite pulse generator based on full-bridge inverter and soft switching for biological applications," *IEEE Trans. Dielectr. Elect. Insul.*, vol. 23, no. 5, pp. 2730–2737, Oct. 2016.

[10] X. Song, A. Q. Huang, S. Sen, L. Zhang, P. Liu, and X. Ni, "15-kV/40-A FREEDM supercascode: A cost-effective SiC high-voltage and high-frequency power switch," *IEEE Trans. Ind. Appl.*, vol. 53, no. 6, pp. 5715–5727, Nov./Dec. 2017.
[11] L. Pang, T. Long, K. He, Y. Huang, and Q. Zhang, "A compact series-connected SiC MOSFETs module and its application in high voltage nanosecond pulse generator," *IEEE Trans. Ind. Electron.*, vol. 66, no. 12, pp. 9238–9247, Dec. 2019.
[12] L. Li, J. Yan, S. Shen, and W. Ding, "A bipolar high voltage pulse generator used for irreversible electroporation ablation," in *Proc. IEEE Pulsed Power Plasma Sci.*, Orlando, FL, USA, 2019, pp. 1–4.
[13] X. Zhang and G. Li, "High-frequency bipolar pulse power supply based on improved Marx generator for medical applications," in *Proc. IEEE 9th Int. Power Electron. Motion Control Conf.*, Nanjing, China, 2020, pp. 2505–2508.
[14] X. Lan, M. Long, X. Zi-jie, X. Qin, Z. De-qing, and Y. Zi-kang, "A novel generator for high-voltage bipolar square pulses with applications in sterilization of microorganism," *IEEE Trans. Dielectr. Elect. Insul.*, vol. 22, no. 4, pp. 1887–1895, Aug. 2015.
[15] A. A. Elserougi, I. Abdelsalam, A. M. Massoud, and S. Ahmed, "A full-bridge submodule-based modular unipolar/bipolar high-voltage pulse generator with sequential charging of capacitors," *IEEE Trans. Plasma Sci.*, vol. 45, no. 1, pp. 91–99, Jan. 2017.
[16] S. Jiang *et al.*, "A bipolar modular multilevel generator based on half-bridge and special full-bridge for electroporation applications," *IEEE Trans. Plasma Sci.*, vol. 49, no. 6, pp. 1920–1927, Jun. 2021.
[17] W. Zeng *et al.*, "A novel high-frequency bipolar pulsed power generator for biological applications," *IEEE Trans. Power Electron.*, vol. 35, no. 12, pp. 12861–12870, Dec. 2020.
[18] Y. Mi, J. Chen, N. Xu, and J. Dai, "High frequency nanosecond pulse generator based on modular multilevel converter structure with auxiliary charging branch," *Trans. China Electrotech. Soc.*, vol. 36, no. 2, pp. 435–444, 2021.
[19] Y. Liu, R. Fan, X. Zhang, Z. Tu, and J. Zhang, "Bipolar high voltage pulse generator without H-bridge based on cascade of positive and negative Marx generators," *IEEE Trans. Dielectr. Elect. Insul.*, vol. 26, no. 2, pp. 476–483, Apr. 2019.
[20] Y. Mi, H. Wan, C. Bian, W. Peng, and L. Gui, "n MMC-based modular unipolar/bipolar high-voltage nanosecond pulse generator with adjustable rise/fall time," *IEEE Trans. Dielectr. Electr. Insul.*, vol. 26, no. 2, pp. 515–522, Apr. 2019.
[21] Y. Mi, C. Bian, P. Li, C. Yao, and C. Li, "A modular generator of nanosecond pulses with adjustable polarity and high repetition rate," *IEEE Trans. Power Electron.*, vol. 33, no. 12, pp. 10654–10662, Dec. 2018.
[22] P. Butkus, A. Murauskas, S. Tolvaisiene, and V. Novickij, "Concepts and capabilities of in-house built nanosecond pulsed electric field (nsPEF) generators for electroporation: State of art," *Appl. Sci.-Basel*, vol. 10, no. 12, Jun. 2020, Art. no. 4244.
[23] W. Jiang, H. Sugiyama, and A. Tokuchi, "Pulsed power generation by solid-state LTD," *IEEE Trans. Plasma Sci.*, vol. 42, no. 11, pp. 3603–3608, Nov. 2014.
[24] M. R. Kazemi, T. Sugai, A. Tokuchi, and W. Jiang, "Waveform control of pulsed-power generator based on solid-state LTD," *IEEE Trans. Plasma Sci.*, vol. 45, no. 2, pp. 247–251, Feb. 2017.
[25] J. Rao, Y. Zhu, Y. Wang, S. Jiang, and Z. Li, "Study on the basic characteristics of solid-state linear transformer drivers," *IEEE Trans. Plasma Sci.*, vol. 48, no. 9, pp. 3168–3175, Sep. 2020.
[26] W. Jiang, "Review of solid-state linear transformer driver technology," *Matter Radiat. Extremes*, vol. 3, no. 4, pp. 159–164, May 2018.
[27] E. Pirc, B. Balosetti, D. Miklavcic, and M. Rebersek, "Electronic emulator of biological tissue as an electrical load during electroporation," *Appl. Sci.-Basel*, vol. 10, no. 9, p. 3103, May 2020.
[28] Y. Chen, J. Du, L. Feng, J. Xiao, J. Zhang, and Y. He, "Comparative study on driving switching characteristics of GaN-FET and SiC-MOSFET in transient high voltage pulse discharge circuit," in *Proc. IEEE Int. Conf. High Voltage Eng. Appl.*, Beijing, China, 2020, pp. 1–4.
[29] Z. Li, A. Bhalla, P. Losee, and K. Zhu, "dV/dt Control methods for UnitedSiC SiC FETs with internal cascode structure," in *Proc. PCIM Europe Digit. Days, Int. Exhib. Conf. Power Electron. Intell. Motion, Renewable Energy Energy Manage.*, Germany: VDE, 2020, pp. 1–7.
[30] B. J. Baliga, *Fundamentals of Power Semiconductor Devices*. New York, NY, USA: Springer, 2012.

Yan Mi (Senior Member, IEEE) was born in Yueyang, China, in 1978. He received the B.S., M.S., and Ph.D. degrees in electrical engineering from Chongqing University, Chongqing, China, in 2000, 2003, and 2009, respectively

He is currently a Professor with the School of Electrical Engineering, Chongqing University. His current research interests include the pulsed power technology and its application in biomedical engineering.

Ning Xu was born in Hengyang, China, in 1997. He received the B.S. degree from China Three Gorges University, Yichang, China, in 2019. He is currently working toward the M.S. degree in electrical engineering with Chongqing University, Chongqing, China.

His research interests include high-repetition-rate pulse power technology.

Jiacheng Chen was born in Harbin, China, in 1995. He received the B.S. degree from the Harbin University of Science and Technology, Harbin, China, in 2018. He is currently working toward the M.S. degree in electrical engineering with Chongqing University, Chongqing, China.

His research interests include pulse power technology.

Zhengmin Li was born in Anhui, China, in 1997. He received the B.S. degree from Hunan University, Changsha, China, in 2020. He is currently working toward the M.S. degree in electrical engineering with Chongqing University, Chongqing, China.

His research interests include high-repetition-rate pulse power technology and application.